Modified minimum-distance criterion for blended random and nonrandom encoding

Markus Duelli, Matthew Reece, and Robert W. Cohn

The ElectroOptics Research Institute, University of Louisville, Louisville, Kentucky 40292

Received December 7, 1998; accepted May 17, 1999; revised manuscript received May 24, 1999

Two pixel-oriented methods for designing Fourier transform holograms—pseudorandom encoding and minimum-distance encoding—usually produce higher-fidelity reconstructions when combined than those produced by each method individually. In previous studies minimum-distance encoding was defined as the mapping from the desired complex value to the closest value produced by the modulator. This method is compared with a new minimum-distance criterion in which the desired complex value is mapped to the closest value that can be realized by pseudorandom encoding. Simulations and experimental measurements using quantized phase and amplitude modulators show that the modified approach to blended encoding produces more faithful reconstructions than those of the previous method. © 1999 Optical Society of America
[S0740-3232(99)02010-4]

OCIS codes: 230.6120, 090.1760, 030.6600, 070.2580.

1. INTRODUCTION

Today the leading methods of designing Fourier transform holograms for laser pattern generation and optical interconnects use iterative search and numerical optimization procedures that vary the modulation values and various degrees of freedom to achieve acceptable diffraction patterns.[1–6] In this prior work it is normally assumed that the design is to be realized as a fixed-pattern diffractive optical element that is subsequently mass produced, which makes computation times of a few minutes to hours[7] insignificant compared with the time required to fabricate the device. However, our previous studies on real-time programmable spatial light modulators (SLM's)[8] and diffractive optical element rapid prototyping systems[9] have led us to reconsider the design problem with particular emphasis on significantly reducing the design time.

By far, the fastest design algorithms are those that directly map a desired complex-valued function into a transmittance function that can be physically produced by the available modulator. The delayed-sampling method of Brown and Lohmann is one of the earliest applications in optics of this idea.[10] The numerical speed of this and many other mapping/encoding methods that were evaluated in the first decade of computer-generated holography[11,12] is due to serial encoding of each desired complex value into a corresponding value of transmittance. Since the various degrees of freedom are not included in this design approach (e.g., in the design of most spot array generators, where the phase of the far-field diffraction pattern is usually not of concern), the performance of the encoding method in terms of diffraction efficiency or other related metrics can be substantially less than that for the optimization methods. Nonetheless, we believe that there are applications that would benefit from the faster encoding algorithms (for example scenarios see Ref. 13).

To reduce the differences in performance between optimal designs and encoded designs, we have begun investigating suboptimal design strategies in which some additional computations (but fewer than those required to find the global optimum) are directed at improving device performance.[14,15] Two possible suboptimal strategies are (1) to use the best solution found by optimization for a given amount of time or (2) to optimize by using some, rather than all, of the available design freedoms. It is this second approach that we consider here.

Specifically, we consider encoding methods that can be improved by varying a single design freedom/free parameter. The free parameter (referred to as γ) scales the magnitude of the complex-valued function that is to be encoded. Each value of the complex function is encoded by one of two encoding algorithms: pseudorandom encoding (PRE)[16] for smaller-magnitude values and minimum-distance encoding (MDE)[17] for larger values, both of which will be reviewed in Sections 2 and 3. Increasing the value of the free parameter decreases the number of complex values that are encoded by the PRE algorithm and increases the number of values encoded by the MDE algorithm. In this way the free parameter controls the blending of the two encoding algorithms.

Designs by this approach have been described in a nonarchival conference proceedings[14] and in brief detail in a short paper.[15] In each specific design considered, it was found that better performance is achieved over PRE or MDE individually by blending the two algorithms and that there is a particular degree of blending (as measured by γ) that gives the best performance of all blendings. At times we have noted dramatic improvements in performance even if only a few percent of the complex values are encoded by MDE.[14] However, we recently observed for modulators that produce only three quantized values of phase that the blending of MDE and PRE leads to only slight performance improvements, and for some blendings the performance is even lower than that without blending.

0740-3232/99/102425-14$15.00

This observation leads us in this paper to propose, consider, and evaluate a modified blending of encoding algorithms. Figure 1(a) shows the phase-only SLM characteristic that was considered in Refs. 14 and 15. Desired complex values that are inside the phase-only modulation characteristic (striped region) can be pseudorandom encoded. The values outside the region are mapped to the closest point on the modulation characteristic (along radial lines centered on the origin).

There is an alternative possible mapping that becomes apparent when considering blended encoding with noncircular SLM characteristics. This is illustrated in Fig. 1(b) for a tri-phase SLM. The striped region again represents the range of values that can be encoded by the PRE algorithm. There are now two possible minimum-distance mappings. The conventional MDE algorithm[17] maps the desired value to the closest value produced by the SLM. Alternatively, we propose a modified MDE (mMDE) in which the desired value is first mapped to the closest value that can be pseudorandom encoded, and then the mapped value is encoded to a modulation value by PRE.

In this paper we will show, by using both computer simulations and experiments with a phase-only SLM, that the proposed modified blended encoding algorithm generally outperforms the earlier blended algorithm in terms of two metrics that describe fidelity of the reconstruction (the ratio of intensity of the desired portions of the diffraction pattern to peak background noise and the relative error in intensity between the desired and actual diffraction patterns). This demonstration is the primary objective of this paper. One secondary objective is to suggest how blended encoding algorithms can be developed for a variety of SLM modulation characteristics. Our approach is to develop blended algorithms for several different modulation characteristics. Another secondary objective is to provide a comprehensive comparison of the performance of various encoding algorithms developed to date. This is achieved by encoding an identical desired function for each algorithm and for each value of the scaling parameter γ.

Section 2 reviews the development of the proposed encoding algorithm and presents general background that is used to develop the new algorithms. Section 3 defines the modulation characteristics and the algorithms used in the study. Section 4 reports the results of the simulation study, and Section 5 presents the experimental results.

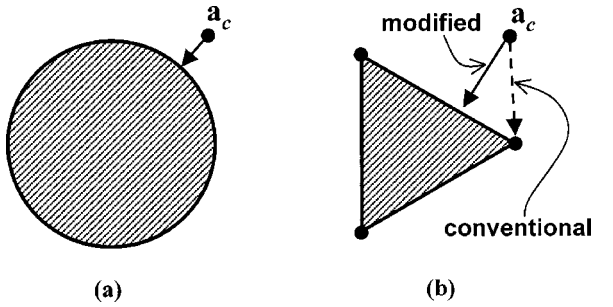

Fig. 1. Modulation characteristics for which the minimum-distance mapping to the modulation characteristic and to the encoding range (striped regions) of the PRE algorithm are (a) identical and (b) different. In (a) the modulation characteristic is a circle, and in (b) the modulation characteristic is the three dots, one at each apex of the triangle.

2. BACKGROUND ON AND REVIEW OF ENCODING

A. Review of Pixel-Oriented Encoding Algorithms

The design methods considered in this paper can be classified as pixel-oriented encoding, since each pixel represents a desired complex value independent of the values represented by all other pixels in the SLM.[18] Pixel-oriented encoding is a special case of point-oriented encoding. In traditional point-oriented encoding methods, the desired complex-valued function is modulated onto a carrier of spatial frequency that exceeds the space–bandwidth product (SBWP) of the desired complex function.[11,12,19] Therefore these methods require SLM's with SBWP's that exceed the SBWP of the desired signal. However, in pixel-oriented encoding the SBWP of the signal can be as large as that of the SLM as a result of the one-for-one mapping between each desired complex value and the modulation value of each corresponding pixel. Thus pixel-oriented encoding has an advantage over traditional point-oriented encoding, and also group-oriented encoding methods,[9,11,12] when the SLM has a small number of pixels, as is the case for most of the electrically addressable SLM's that are available today.

There appear to be two approaches to pixel-oriented encoding. One approach is to map each desired complex value to the closest available modulation value produced by its corresponding pixel.[17] For continuous-value phase-only SLM's this prescription leads to a unique mapping in which the amplitude of each value is set to unity and the mapped phase is identical with the desired phase. That is, MDE for the continuous-value phase-only SLM reduces to the well-known kinoform[20] or phase-only filter.[21]

The second encoding approach, PRE,[16,22] rather than selecting the closest available modulation value, selects one modulation value from a range of possible values by using a computer-generated random (i.e., pseudorandom) number. The statistical properties of the random-number generator are designed so that the average modulation value is identical with the desired complex value. The diffraction pattern produced by this transmittance function has an average intensity that is identical with the desired diffraction pattern plus a noise background. The diffraction efficiency η of the pseudorandom-encoded function is identical with that of the desired fully complex function. The remaining energy $1 - \eta$ is either scattered into the noise background for phase-only SLM's or scattered into noise and absorbed if the SLM is non-phase-only.

PRE differs from MDE in that MDE always maps the desired value to the closest available value on the modulation characteristic while PRE maps the desired value to closer modulation values with greater relative frequency than to modulation values that are farther away. For quantized modulation characteristics the encoding algorithms are analogous to the numerical rounding of floating-point numbers. MDE is analogous to nearest-integer rounding, while PRE corresponds to rounding to the nearest integer most frequently and to the furthest integer least frequently according to a random selection process. MDE and PRE are illustrated in Fig. 2 for tri-phase modulation (with modulation values $\mathbf{a}_{m1}$, $\mathbf{a}_{m2}$, and

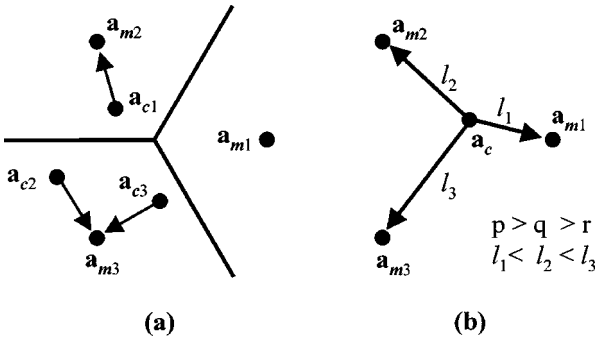

Fig. 2. Comparison of (a) the MDE algorithm with (b) the PRE algorithm for a tri-phase phase-only modulation characteristic.

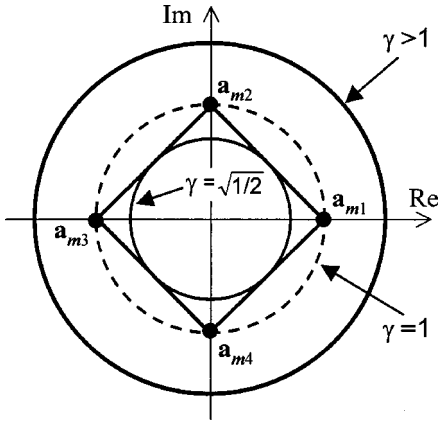

Fig. 3. Illustration of the encoding range and the fully complex encoding range, and their relationship to the scaling parameter γ for a quad-phase modulation characteristic.

$\mathbf{a}_{m3}$). For MDE [Fig. 2(a)], mapping to the closest value of modulation divides the complex plane into three decision regions separated by the three lines. For PRE [Fig. 2(b)] the modulation values $\mathbf{a}_{m1}$, $\mathbf{a}_{m2}$, and $\mathbf{a}_{m3}$ are randomly selected with the relative frequencies/probabilities p, q, and r (which are inversely proportional to l_1, l_2, and l_3, the distances between the desired value $\mathbf{a}_c$ and the modulator values). The complete mathematical specification of these PRE and MDE algorithms for tri-phase modulation and various other modulation characteristics are given in Section 3. The PRE algorithms for quantized modulation were originally derived and compared with MDE algorithms for quantized modulation in Ref. 22.

B. Review of Reduced-Parameter Suboptimal Design Methods

The earliest applications of design optimization using a few parameters appear in the work of Farn and Goodman[23] and in Juday[17,24] on the design of single-object correlation filters for limited-modulation-range SLM's.[17,23,24] Reference 17 presents this problem in its most general form. A fully complex filter is specified that optimizes a given performance metric. The filter has the complex-valued free parameter $\mathbf{\Gamma} = \gamma \exp(j\beta)$, which scales the amplitude of the desired function by γ and rotates the phase by β. The desired function is encoded by the MDE algorithm for different values of γ and β. The optimal values γ^* and β^* minimize the sum of squares error between the desired function and the encoded values. There are no other free parameters for the single-object matched filter, and thus the design is optimal. However, more recent studies have reported suboptimal searches over these two parameters for the design of composite pattern recognition filters[25] and spot array generators.[26] These studies predated and stimulated the development of the first algorithms that blend MDE and PRE to various degrees as a function of the free parameter γ.[14,15]

In specific cases searches over one or both of the free parameters can be avoided. For specific modulation characteristics the encoding algorithm can be independent of γ and/or β. For instance, in Fig. 2(a), the sum of squares error for MDE is independent of γ but dependent on β. As stated in Section 1, for continuous-value phase-only SLM's the MDE algorithm reduces to the classical kinoform, and thus no search is required at all. Also, the distribution of the desired values over the complex plane can make the optimization insensitive to the variation in γ or β. For instance, in Fig. 2, if the desired complex values are uniformly distributed in magnitude and phase, then there is essentially no dependence on the value of β. This observation is used in the present study to perform single-parameter searches over γ for both MDE and blended encoding.

C. Pseudorandom Encoding Range and Fully Complex Encoding Range

Another reason for the development of blended algorithms is that while MDE algorithms can encode complex values of any magnitude, the PRE algorithm cannot.[27] This is because in PRE the desired value is encoded so that its complex value is equivalent to an average of the available modulation values, and the average is thus constrained to lie between the modulation values. A procedure for evaluating the range over the complex plane that can be encoded by a given PRE algorithm is developed in Ref. 27. Ranges for the modulation characteristics considered in this paper are shown in Figs. 1 and 3. For continuous phase-only modulation [Fig. 1(a)], the PRE range is the interior of the unit circle. Figure 1(b) shows the range for three-value quantized phase modulation. The encoding for the PRE algorithm is the triangular region that is enclosed by the line segments connecting the three values of modulation. Similarly, for a four-value quantized phase modulation (Fig. 3), the encoding range is the square and its interior, which is defined by the line segments connecting the modulation values.

Note that in Fig. 3 the desired complex function can be normalized so that its values are contained within a circle of radius $\gamma = \sqrt{1/2}$. We refer to this as the fully complex encoding range for the quantized PRE algorithm. (For individual functions for which the distribution of complex values is noncircular, the fully complex range can approach $\gamma = 1$. However, we apply this definition not to individual functions but rather to the set of all functions of interest.) Also note that for phase-only modulation the encoding range and the fully complex range are identical (the region enclosed by $\gamma = 1$ in Fig. 3) and that they enclose a larger area of the complex plane than does the

quantized PRE algorithm. In this paper the encoding range is increased by blending PRE algorithms with algorithms that do not have limited encoding ranges. As shown in Sections 4 and 5, the diffraction efficiency is increased and the fidelity is optimized for fully complex encoding ranges (as designated by the scaling parameter γ) that exceed the encoding range of PRE alone.

3. DESIGN OF THE STUDY

A. Modulation Characteristics

The modulation characteristics considered in this study are illustrated in Fig. 4. Three of the characteristics [(a)–(c)] are phase only: (a) continuous, (b) three phases uniformly spaced around the unit circle, and (c) four uniformly spaced phases. Adding an additional zero value to each characteristic gives the bi-amplitude modulation characteristics [(d)–(f)]. We will refer to these modulation characteristics by using the descriptive terms tri-phase and quad-phase. Also, we use the terms bi-amplitude phase and phase-only to distinguish between modulation characteristics that have or do not have a zero value.

B. Encoding Algorithms

The implementation and the theory of PRE and MDE have been presented in the publications reviewed in Sections 1 and 2. We present only the details necessary to permit others to understand and to reproduce the results presented in Sections 4 and 5. As an aid to the reader, each of the specific algorithms studied is presented in the figures. We begin with the less-involved algorithms for the continuous modulation characteristics [Figs. 4(a) and 4(d)] and proceed through increasingly involved algorithms for tri-phase [Figs. 4(b) and 4(e)] and quad-phase [Figs. 4(c) and 4(f)] characteristics.

C. Encoding Algorithms for Continuous Spatial Light Modulators

Figure 5(a) illustrates MDE for a phase-only SLM. As mentioned in Subsection 2.B because of circular symmetry of the modulation characteristic the desired fully complex function [illustrated by the values $\mathbf{a}_{c1}$ and $\mathbf{a}_{c2}$ in Fig. 5(a)] can be scaled by an arbitrary complex number $\mathbf{\Gamma}$ and the encoding still maps to the unit circle identically. However, with the addition of a zero value of modulation MDE for the bi-amplitude phase modulator, the mapping becomes more involved in two respects: (1) While the mapping is still along radial lines, there is now a threshold level [dashed curve in Fig. 5(d)]. Values less than radius 1/2 are closer to the origin than to unity and therefore map to the origin. (2) Because of the threshold the mapping now depends on the magnitude of the scaling parameter γ. For $\gamma = 0$ all the desired complex values map to $\mathbf{a}_0$, and for $\gamma = \infty$ the complex values map to the unit circle, which is identical with the mapping in Fig. 5(a).

Our convention for reporting the value of the scaling parameter γ (for all encoding algorithms presented) is as follows: The desired complex function consists of N samples $\mathbf{a}_{ci}$ at positions indexed by i from 1 to N. The complex values are normalized so that the maximum value of $|\mathbf{a}_{ci}|$ from the N samples is identical with γ. The value of γ that produces the best performance according to a given metric or cost function is usually written as γ^*.

Figure 5(b) illustrates PRE for phase-only SLM's. This particular algorithm was introduced in Ref. 22. The desired value $\mathbf{a}_{c1}$ is mapped to one of two modulation values that are 180° apart. For each pixel transmittance

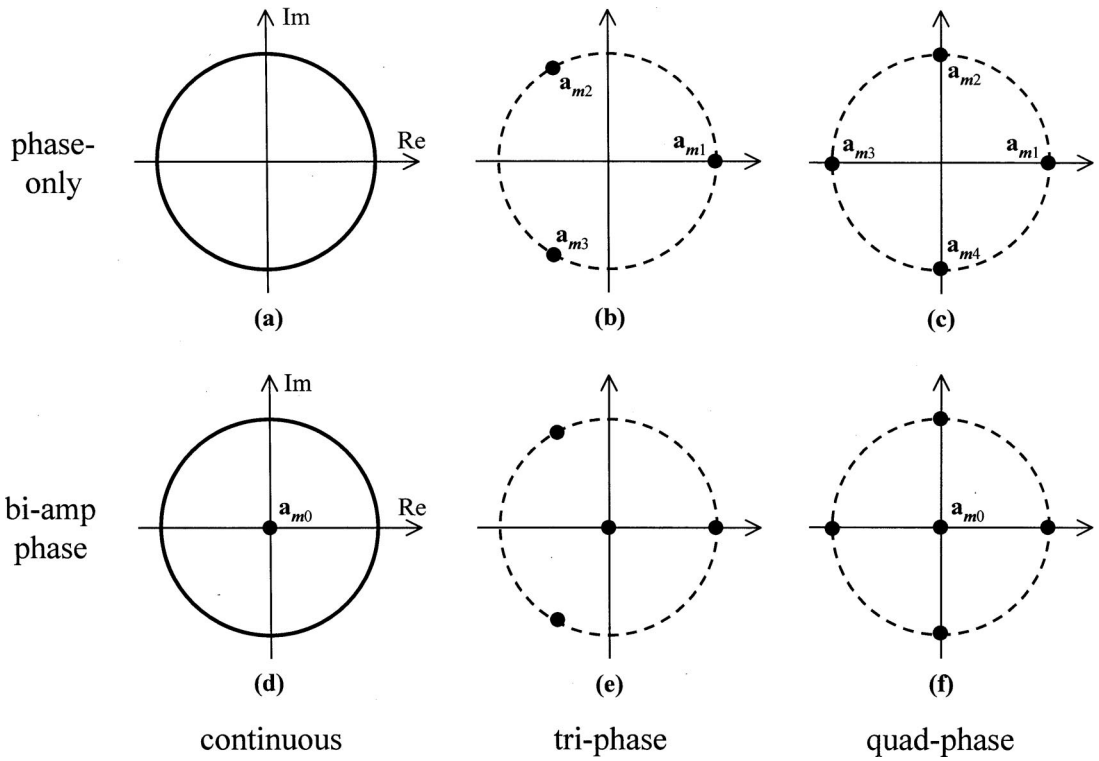

Fig. 4. Classification of the various modulation characteristics considered in this paper.

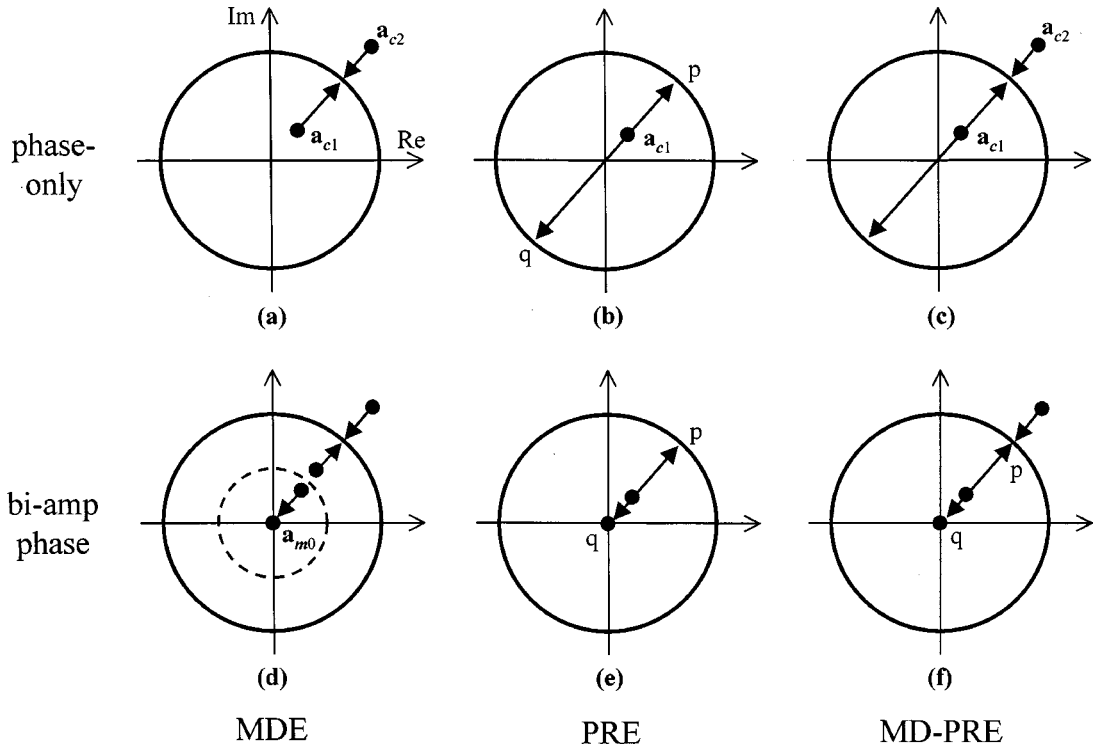

Fig. 5. Illustration of the individual MDE and PRE algorithms together with their blending for continuous modulation characteristics.

$\mathbf{a}_{ci}$, the probability of selecting the modulation value that is closer to the desired value is

$$p_i = (1 + |\mathbf{a}_{ci}|)/2, \tag{1}$$

and the probability of selecting the alternative value is $q_i = 1 - p_i$. With these values of probability, the encoding formula is

$$\mathbf{a}_i = \begin{cases} \exp[j \arg(\mathbf{a}_{ci})] & \text{if } 0 \leqslant s_i < p_i \\ -\exp[j \arg(\mathbf{a}_{ci})] & \text{if } p_i \leqslant s_i \leqslant 1 \end{cases}, \tag{2}$$

where $\mathbf{a}_i$ is the actual modulation selected for the ith modulator pixel and s_i is a computer-generated random number uniformly distributed between 0 and 1. To reduce encoding errors, one usually tries to make the value of γ as large as possible.[27] For phase-only SLM's this corresponds to $\gamma = 1$. For values of $\gamma > 1$ the complex values that exceed unity cannot be pseudorandom encoded. These values can be encoded by MDE, which leads to the blended minimum-distance and pseudorandom encoding algorithm (MD-PRE) illustrated in Fig. 5(c).

The PRE algorithm for bi-amplitude phase modulation is illustrated in Fig. 5(e). The probability is

$$p_i = |\mathbf{a}_{ci}|, \tag{3}$$

and $q_i = 1 - p_i$. The encoding formula is

$$\mathbf{a}_i = \begin{cases} \exp[j \arg(\mathbf{a}_{ci})] & \text{if } 0 \leqslant s_i < p_i \\ 0 & \text{if } p_i \leqslant s_i \leqslant 1 \end{cases}. \tag{4}$$

The MD-PRE algorithm for bi-amplitude phase modulation [Fig. 5(f)] uses the PRE algorithm for encoding values inside the unit circle and phase-only MDE for encoding values outside the unit circle.

D. Ternary Pseudorandom Encoding

The encoding formula for ternary-valued modulation[22] is presented here in general form because it is the basis for the PRE algorithms for all the quantized SLM's considered in this study [Figs. 4(b), 4(c), 4(e), and 4(f)]. The ternary PRE algorithm can be specified for any three modulation values $\mathbf{a}_{m1}$, $\mathbf{a}_{m2}$, and $\mathbf{a}_{m3}$ as long as they do not lie on a common line. The encoding formula is

$$\mathbf{a}_i = \begin{cases} \mathbf{a}_{m1} & \text{if } 0 \leqslant s_i < p_i \\ \mathbf{a}_{m2} & \text{if } p_i \leqslant s_i < 1 - r_i, \\ \mathbf{a}_{m3} & \text{if } 1 - r_i \leqslant s_i \leqslant 1 \end{cases} \tag{5}$$

where p_i is the probability of selecting $\mathbf{a}_{m1}$, q_i is the probability of selecting $\mathbf{a}_{m2}$, and r_i is the probability of selecting $\mathbf{a}_{m3}$. As in Subsection 3.C, s_i is a random number drawn from the uniform probability distribution. The three probabilities are found by solving

$$\begin{pmatrix} \mathrm{Re}(\mathbf{a}_{ci}) \\ \mathrm{Im}(\mathbf{a}_{ci}) \\ 1 \end{pmatrix} = \begin{bmatrix} \mathrm{Re}(\mathbf{a}_{m1}) & \mathrm{Re}(\mathbf{a}_{m2}) & \mathrm{Re}(\mathbf{a}_{m3}) \\ \mathrm{Im}(\mathbf{a}_{m1}) & \mathrm{Im}(\mathbf{a}_{m2}) & \mathrm{Im}(\mathbf{a}_{m3}) \\ 1 & 1 & 1 \end{bmatrix} \begin{pmatrix} p_i \\ q_i \\ r_i \end{pmatrix}, \tag{6}$$

where $\mathbf{a}_{ci}$ is the desired complex value that is encoded. For quantized SLM's that have more than three modulation values, the PRE algorithm is developed by using Eqs. (5) and (6) with various groups of three modulation values to encode various regions of the complex plane.

E. Encoding Algorithms for Quantized Phase-Only Spatial Light Modulators

Figure 6 illustrates how the individual MDE and PRE algorithms are combined into the MD-PRE and modified

MD-PRE (mMD-PRE) algorithms for both tri-phase and quad-phase modulation characteristics.

For MDE on tri-phase SLM's, the complex plane is divided into three decision regions [Fig. 6(a)], and desired values in a particular region are mapped to the modulation value in that region. For PRE on tri-phase SLM's [Fig. 6(b)], the modulation values used in Eqs. (5) and (6) are $\mathbf{a}_{m1} = 1$, $\mathbf{a}_{m2} = \exp(j2\pi/3)$, and $\mathbf{a}_{m3} = \exp(-j2\pi/3)$. Values in the interior of the triangle in Fig. 6(b) can be pseudorandom encoded, and the inscribed circle (dashed curve), which is of radius $\gamma = 0.5$, represents the fully complex range for this PRE algorithm. The MD-PRE blended algorithm uses PRE for desired values on and inside the triangle of Fig. 6(b), and it uses the MDE decision regions of Fig. 6(a) for values outside the triangle. The PRE and MDE regions for the blended algorithms are labeled in Fig. 6(c).

As in Fig. 1(b), MD-PRE can be modified to the mMD-PRE algorithm by mapping desired values that are outside the PRE range to the closest values on the boundary of the PRE range. Then the mapped value is encoded by the PRE algorithm. We will refer to the mapping of values by this prescription as modified MDE (mMDE). The mMDE regions are identified in Fig. 6(d). The regions identified as MDE in Fig. 6(d) are also encoded by the mMDE prescription; however, mMDE for these regions is identical with MDE.

The mMD-PRE for the quad-phase SLM is developed in a similar manner to that described for tri-phase encoding. Figures 6(e)–6(h) illustrate the corresponding succession of steps for the quad-phase SLM. Note that for the quad-phase PRE algorithm the fully complex range becomes $\gamma = \sqrt{1/2}$, as indicated by the dashed curve in Fig. 6(f). Also note that Fig. 6(f) distinguishes between two regions in the encoding range of the PRE algorithm. For each region a tri-phase PRE algorithm is used. If $\mathbf{a}_{ci}$ is in region I, then it is encoded by using the modulation values $\mathbf{a}_{m1} = 1$, $\mathbf{a}_{m2} = j$, and $\mathbf{a}_{m3} = -1$, and if $\mathbf{a}_{ci}$ is in region II, then it is encoded by using $\mathbf{a}_{m1} = 1$, $\mathbf{a}_{m4} = -j$, and $\mathbf{a}_{m3} = -1$. The encoding formula can be written as

$$\mathbf{a}_i = \begin{cases} 1 & \text{if } 0 \leqslant s_i < p_i \\ \pm j & \text{if } p_i \leqslant s_i < 1 - r_i, \\ -1 & \text{if } 1 - r_i \leqslant s_i \leqslant 1 \end{cases} \tag{7}$$

where in the second line j is used if $\mathbf{a}_{ci}$ is in region I and $-j$ is used if $\mathbf{a}_{ci}$ is in region II. The values of probability used in Eq. (7) are determined by solving the equation

$$\begin{pmatrix} \mathrm{Re}(\mathbf{a}_{ci}) \\ \mathrm{Im}(\mathbf{a}_{ci}) \\ 1 \end{pmatrix} = \begin{bmatrix} 1 & 0 & -1 \\ 0 & \pm 1 & 0 \\ 1 & 1 & 1 \end{bmatrix} \begin{pmatrix} p_i \\ q_i \\ r_i \end{pmatrix}, \tag{8}$$

where $+1$ is used if $\mathbf{a}_{ci}$ is in region I and -1 is used if $\mathbf{a}_{ci}$ is in region II.

F. Encoding Algorithms for Quantized Biamplitude Phase Spatial Light Modulators

Figure 7 identifies the various encoding regions for PRE and MDE with the addition of the modulation value $\mathbf{a}_{m0} = 0$. For both tri-phase MDE [Fig. 7(a)] and quad-phase MDE [Fig. 7(c)], one additional decision region is formed. For PRE on the tri-phase SLM, there are three regions, each of which is pseudorandom encoded by using the

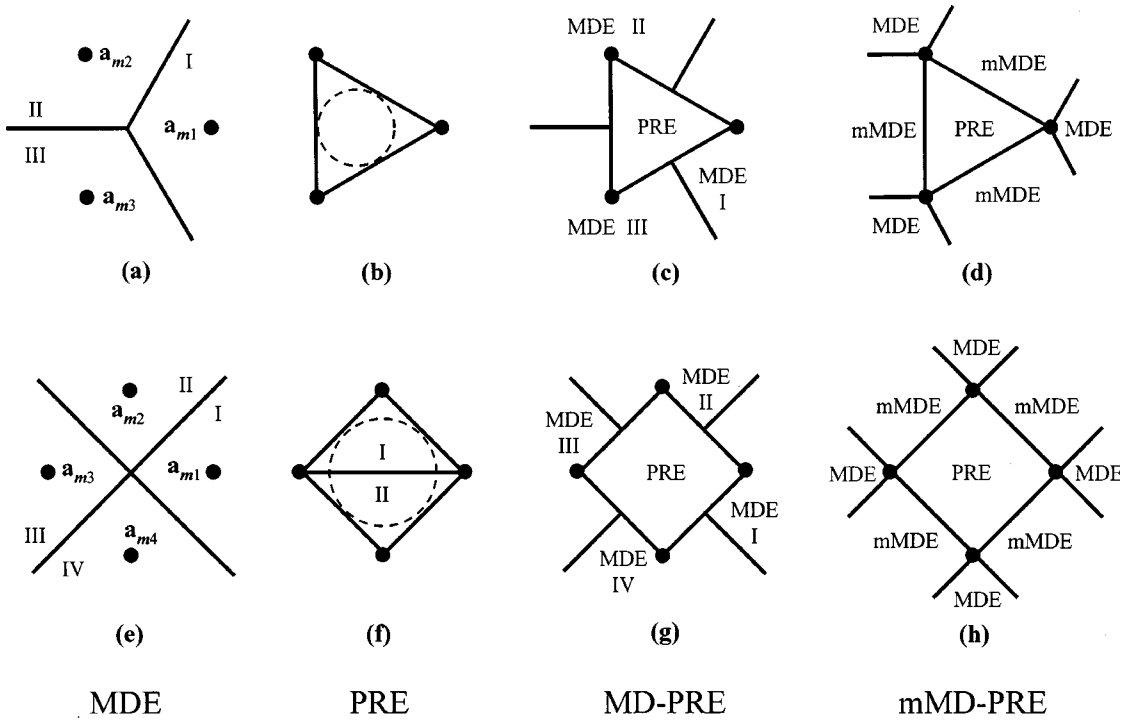

Fig. 6. Illustration of the individual MDE and PRE algorithms together with their minimum-distance and modified-minimum-distance blendings for [(a)–(d)] tri-phase and [(e)–(h)] quad-phase phase-only modulation characteristics. Parts (a) and (e) identify the decision regions for MDE. Parts (b) and (f) show the encoding ranges for the PRE algorithms together with the fully complex ranges, which are bounded by each dashed circle. Part (f) also indicates that there are two regions. Each triangular region is encoded by Eqs. (7) and (8) with use of the three modulation values at the corners of the corresponding regions.

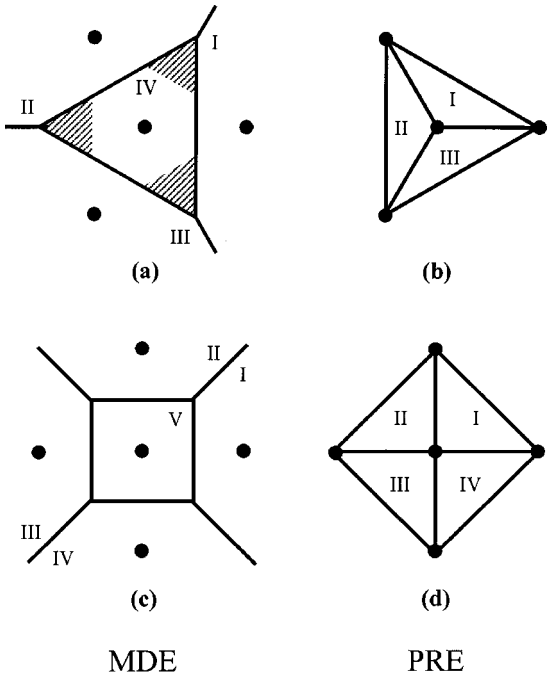

Fig. 7. Illustration of the individual MDE and PRE algorithms for bi-amplitude modulation characteristics: (a) MDE and (b) PRE for tri-phase SLM's; (c) MDE and (d) PRE for quad-phase SLM's. Parts (a) and (c) show the decision regions for the MDE algorithms. Parts (b) and (d) show the individual subregions that are each encoded by using ternary PRE. The striped areas of region IV in (a) are outside the encoding range for PRE in (b). Therefore the MD-PRE blending of (a) and (b) requires that values in the striped areas be mapped to zero according to the MDE algorithm.

modulation values $\mathbf{a}_{m0} = 0$ and two of the three other values $\mathbf{a}_{m1}$, $\mathbf{a}_{m2}$, and $\mathbf{a}_{m3}$ in Fig. 7(b). Similarly, for PRE with a quad-phase SLM there are four regions, each of which is pseudorandom encoded by using Eqs. (5) and (6) with $\mathbf{a}_{m0}$ and two of the four other values $\mathbf{a}_{m1}$, $\mathbf{a}_{m2}$, $\mathbf{a}_{m3}$, and $\mathbf{a}_{m4}$ in Fig. 7(d).

Even though the PRE algorithms used for the quantized bi-amplitude SLM's are different from those used for the quantized phase-only SLM's, the encoding ranges of the PRE algorithms are identical. This leads to the PRE and MDE regions for the blended algorithms being identical with those for the phase-only SLM's [Figs. 6(c), 6(d), 6(g), and 6(h)], with one exception [Fig. 6(c)]. From Figs. 7(c) and 7(d), it can be seen that MDE region V is entirely contained inside the PRE encoding range, and thus this region is always encoded by PRE and is never encoded by MDE. Therefore Figs. 6(g) and 6(h) apply to the bi-amplitude SLM as well. However, Figs. 7(a) and 7(b) show that some of MDE region IV (the three striped regions) are outside the encoding range for PRE. Therefore the three striped regions should be added onto Fig. 6(c) to properly describe the encoding regions for MD-PRE for the tri-phase bi-amplitude SLM. For mMD-PRE the mMDE regions take precedence over the MDE IV regions, and thus Fig. 6(d) describes the encoding range for both the phase-only and the bi-amplitude SLM.

In passing, we note that for MD-PRE on tri-phase bi-amplitude SLM's there is a dramatic difference between encoding a value in the PRE region and in the MDE IV regions that are outside the PRE region. Desired values in the PRE region are mapped on a percentage basis to one of the three closest SLM values, while values in the MDE IV region are always mapped to zero. This algorithm has led to the somewhat paradoxical result that some values further from zero are mapped to zero more frequently than other values that are closer to zero.

G. Specification of the Desired Function To Be Encoded

The desired function that is encoded is written in the form

$$\mathbf{a}_c(x, y) = \sum_{k=1}^{7} \exp(j\theta_k)\exp(j2\pi kx) \times \sum_{l=1}^{7} \exp(j\theta_l)\exp(j2\pi ly), \tag{9}$$

where θ_k are the phases specified by Krackhardt *et al.* for a maximum-diffraction-efficiency, phase-only 1×7 spot array.[28] Equation (9), which is periodic, is sampled to produce a 32×32 unit cell of complex values, and from this a 4×4 array of cells is adjoined to produce the array of 128×128 desired complex values.

Neither PRE nor blended encoding requires that the desired function be designed by optimization. Nor were optimized functions encoded in Refs. 14 and 15. However, it is useful to use Eq. (9) because this function and its performance are well-known and because it provides information that relates the performance of encoding procedures to the performance of optimized designs.

Since Eq. (9) is periodic, one might also wonder whether periodic functions have a performance advantage over nonperiodic functions. Reference 15 is the only study of blended algorithms that uses a nonperiodic function. However, several of our studies on PRE alone have identified that the SBWP of the desired function, the diffraction efficiency of the desired function [see Eq. (26) in Ref. 22] and the mean squared distance between the desired function values and the modulation values critically control performance.[22] References 8, 16, and 18, which include simulated and experimental demonstrations using nonperiodic functions, and Ref. 22, which uses periodic functions, all demonstrate similar dependence on these parameters that define the properties of the function.

The encoding of the optimized function suggests that, in addition to design, the encoding algorithms could also be used to remap an optimized design from one type of modulation characteristic into another. A specific application of remapping would be to use the encoding algorithms for quantized modulation to quantize a continuous-value phase-only diffractive optical element design.

H. Simulation Procedures and Definition of the Performance Metrics

The far-field diffracted intensity patterns are simulated by fast-Fourier-transforming the encoded values $\mathbf{a}_i$ and then squaring the magnitude for each of the pseudorandom and nonrandom encodings. For all metrics except diffraction efficiency, the 128×128 array is placed in a

512×512 array of zeros that is fast Fourier transformed. For diffraction efficiency the 128×128 array is fast Fourier transformed directly. The diffraction efficiency η is simply the sum of the intensities of the 49 spots divided by the sum of all intensities in the 128×128 diffraction pattern. For bi-amplitude modulation characteristics the energy absorption in the modulator plane also needs to be accounted for.[14] Therefore the ratio of desired energy to total energy in the diffraction pattern is multiplied by the ratio of unity-transmittance pixels to the total number of SLM pixels. Nonuniformity of the peaks (NU) is calculated as the standard deviation of the peak intensities of the 49 spots divided by the average spot intensity. Signal-to-peak-noise ratio (SPR) is the ratio of the average peak intensity of the spots to the maximum noise peak of the 512×512 pattern, excluding the square region that contains the 7×7 spot array. Signal-to-noise ratio (SNR) is the ratio of the average intensity of the peak values of each of the 49 spots divided by the average intensity outside the square region containing the 7×7 spot array. SNR is reported for completeness and to provide continuity with the results and the theory on the performance of ternary PRE that was presented in Ref. 22. However, in Section 4 we provide little discussion of the SNR results because SNR does not well characterize the noise in MDE and MD-PRE, which, rather than being white, is localized to a small number of large noise spikes. The calculation of the various metrics from experimental measurements is described in Section 5.

In addition to describing the specific encoding algorithms that are to be evaluated in this study, we hope that our development of these algorithms may serve as examples and suggest how blended encoding algorithms can be developed for the myriad of possible modulation characteristics.

4. SIMULATION RESULTS

This section compares the performance of PRE, MDE, MDE-PRE, and mMDE-PRE algorithms for various modulation characteristics in terms of SPR, NU, and η as a function of the blending/scaling parameter γ and also at selected optimal values of γ^*.

For each encoding performed in this study, the identical desired function $\mathbf{a}_{ci}$ and the 128×128 array of uniform random numbers s_i are used. Using the same random numbers is important because each new set of random numbers used in encoding can affect the value of the performance metrics. However, even using an identical array of random numbers still causes fluctuations in the performance curves. These fluctuations can be reduced by performing the same encoding algorithm multiple times with several sets of random numbers and then averaging together the performance metrics.[8] However, the trends in the performance curves are adequately evident for the purpose of comparing the performance advantages of one algorithm with those of another.

The detailed performance results for the various SLM types are reported below. The first set of results is for continuous SLM's. While there is no distinction between MD-PRE and mMDE-PRE for these characteristics, the results for continuous SLM's provide the clearest demonstration of the improvements that are due to blending and they also provide a baseline against which to compare the performance when the phase characteristic is coarsely quantized.

A. Results for Continuous Spatial Light Modulators

Figure 8 shows the performance as a function of γ for the encoding of the identical function on phase-only and bi-amplitude phase SLM's. MD-PRE for both SLM types is presented together with MDE for the bi-amplitude SLM (which for $\gamma = \infty$ is equivalent to MDE for the phase-only SLM). For each SPR and NU curve, there is a particular value of $1 < \gamma \ll \infty$ for which the performance metric is optimal. The performance metrics for each algorithm when SPR is maximum are reported in Table 1. Since NU is fairly flat in the vicinity of peak SPR, these additional data are not presented. Comparing the curves and

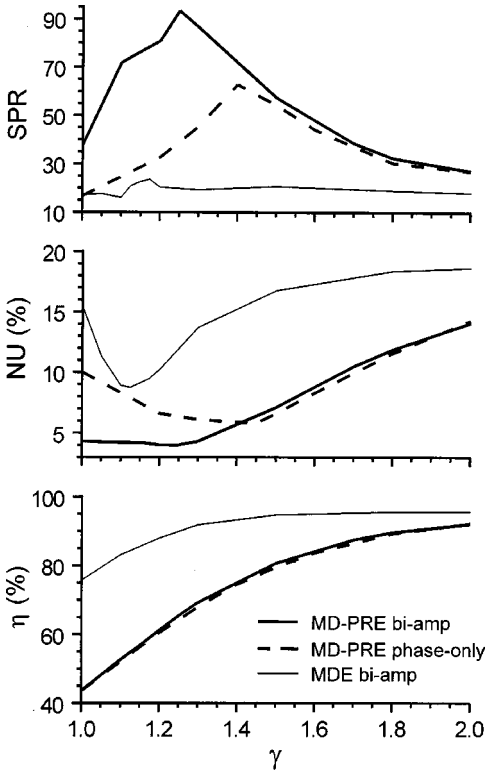

Fig. 8. Simulated performance of blended algorithms as a function of the blending parameter for phase-only and bi-amplitude phase modulation characteristics.

Table 1. Best Performance of Encoding Algorithms for Continuous SLM's

Continuous		Simulation (Experiment)			
Algorithm	γ^*	η (%)	SNR	SPR	NU (%)
Phase-only					
PRE	1.00	44(44)	254 (224)	17(13)	10(15)
MD-PRE	1.40	75(70)	977 (743)	63(43)	6(15)
MDE	∞	96(94)	2263(2135)	20(15)	19(23)
Bi-amplitude					
PRE	1.00	43	685	37	4
MD-PRE	1.25	65	1524	93	4
MDE	1.20	88	7093	20	10

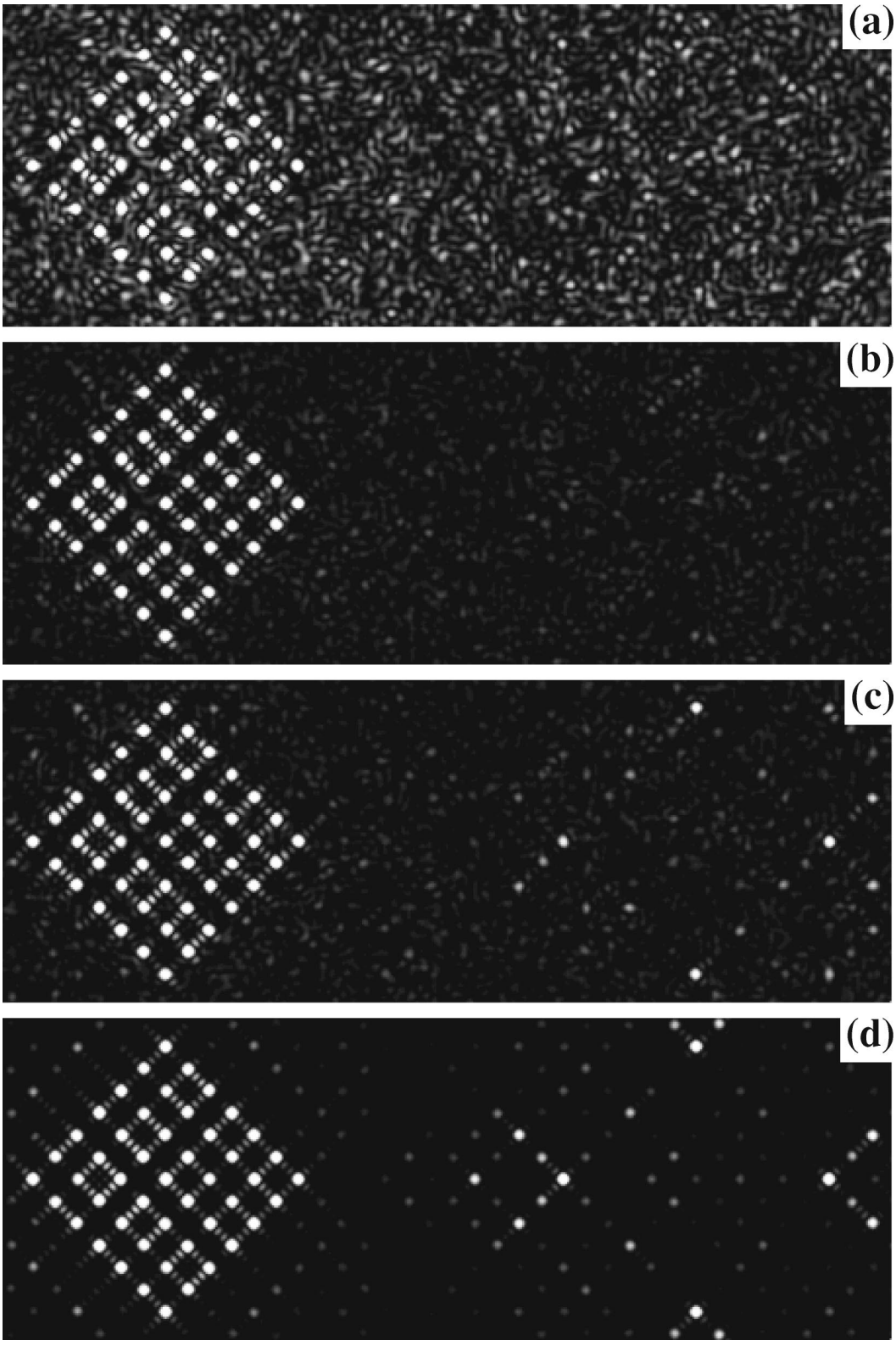

Fig. 9. Simulated far-field intensity patterns of the tri-phase phase-only SLM for (a) PRE, (b) mMD-PRE, (c) MD-PRE, and (d) MDE. The images show intensity with a linear gray scale. To bring out the background noise, the maximum gray-scale value (full white) is 30% of the average intensity of the 49 spots.

table entries with each other, we can also see that MD-PRE for bi-amplitude SLM's outperforms MD-PRE for phase-only SLM's. Both algorithms outperform MDE in SPR and NU. Clearly, MDE produces greater diffraction efficiency; however, the diffraction efficiency for the MD-PRE algorithms can exceed 80% (near $\gamma = 1.6$) and still outperform the best MDE in terms of SPR and NU. The trends in these performance curves are similar to that ob-

served in Ref. 14, where a nonoptimized, lower-diffraction-efficiency function was encoded.

B. Results for Quantized Phase-Only Spatial Light Modulators

The characteristics of the various algorithms and their influence on performance can be appreciated by considering the simulated diffraction patterns of Fig. 9. The values of γ^* used for each type of encoding are reported in Table 2 together with the tabulated performance metrics. The gray scale in Fig. 9 has been set to bring out the structure of the background noise. The background for PRE is a relatively bright speckle pattern [Fig. 9(a)], while the background for MDE is a much different pattern of noise spikes at harmonically related spatial frequencies [Fig. 9(d)]. The background for MD-PRE [Fig. 9(c)] also contains noise spikes having a similar spatial distribution of noise to that for MDE but that are not as bright as those for MDE. There is also a speckle pattern that is quite faint. The background for mMD-PRE [Fig. 9(b)] contains a speckle background that is slightly brighter than the speckle pattern for MD-PRE but that is much less bright than the patterned noise spikes for MD-PRE. There are even patterned noise spikes in Fig. 9(b), but they are faint and obscured to a large degree by the speckle pattern. Figure 9 has been used to show how blending trades off between the background noise properties of PRE and MDE. The cross sections in Fig. 10 of the intensity patterns allow a more quantitative comparison of the performance of the four encoding algorithms. Figure 10 makes clear that it is the appearance of a few very large noise spikes that leads to the low values of SPR for MDE and MD-PRE. Figure 10 also provides a visual comparison of uniformity of the spot arrays. While the mMD-PRE is the most uniform of the four cross sections, the differences are best appreciated by considering the values of NU reported in Table 2 for the uniformity of all 49 spots. The same visual and qualitative distinctions for the four diffraction patterns can be made for encoding with the more finely quantized modulation characteristics [Figs. 4(c), 4(e), and 4(f)] considered in this study. Since noise spikes and the nonuniformity are generally lower, these differences are harder to see and they provide no additional insight into the properties of the encoding algorithms. For this reason the algorithms are compared in terms of their performance metrics in the remainder of the paper.

The performance of the blended encoding algorithms as a function of γ is given in Fig. 11. While the curves are noisier than the continuous curves in Fig. 8, it can be seen that for each SPR curve the maximum value is found for a specific value of γ^* corresponding to a specific blending of PRE and MDE (or mMDE). We have never found a case in which either pure PRE or pure MDE produced a better performance than the blended results. Similarly, for each NU curve, the minimum value corresponds to a specific value of the blending parameter γ^*. Of most significance to this study is that the mMD-PRE curves always attain larger values of SPR and lower values of NU than the corresponding MD-PRE curves. This is true despite the fact that MD-PRE has the larger diffraction efficiency. Rather than reporting the best SPR and the best NU,

Table 2. Best Performance of Encoding Algorithms for Phase-Only SLM's

Phase-Only		Simulation (Experiment)			
Algorithm	γ^*	η (%)	SNR	SPR	NU (%)
Tri-phase					
PRE	0.50	11(11)	40(37)	3(3)	20(23)
MD-PRE	0.80	32(32)	147(152)	2(6)	15(18)
mMD-PRE	0.95	31(28)	147(130)	11(9)	12(15)
MDE	∞	66(57)	411(429)	1(1)	22(25)
Quad-phase					
PRE	0.71	22(18)	93(77)	8(6)	11(14)
MD-PRE	0.95	40(39)	220(196)	13(7)	11(15)
mMD-PRE	1.11	47(45)	290(274)	22(18)	8(14)
MDE	∞	78(77)	1071(949)	4(7)	21(25)

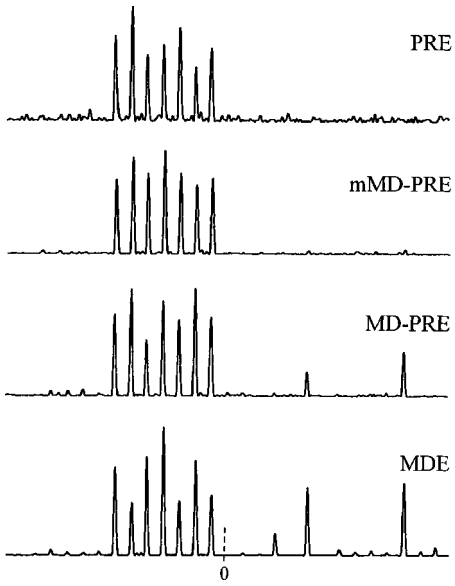

Fig. 10. Cross sections of the far-field intensity patterns of the tri-phase phase-only SLM from Fig. 9. The cross section is taken across the diagonal of the 7×7 spot array and through the optical axis (indicated by the dashed vertical line). The traces are normalized so that the average intensity of each spot array is of identical vertical length on each plot.

Table 2 reports the performance for the best overall combination of SPR and NU (as based on empirical judgment rather than cost function). The selection of the best value of γ^* is not especially critical because NU (or SPR) is slowly varying near its local minimum (or maximum).

C. Results for Quantized Biamplitude Phase Spatial Light Modulators

Figure 12 and Table 3 report these results. Similar trends to those noted for the quantized phase-only SLM's are observed for the biamplitude SLM's. Once again each curve demonstrates that there is a particular degree of blending that produces the best fidelity as measured by SPR or NU. Also, the largest value of SPR for mMD-PRE is always greater than the largest value of SPR for MD-PRE. Similarly, the smallest value of NU for mMD-PRE is always smaller than the smallest value of NU for MD-PRE. The diffraction efficiency for the tri-phase encod-

ings shows that the MD-PRE actually has lower diffraction efficiency than mMD-PRE for $\gamma \lesssim 1$. This reflects the fact that many of the values in the MDE region IV [specifically, the striped regions of Fig. 7(a)] are being mapped to zero.

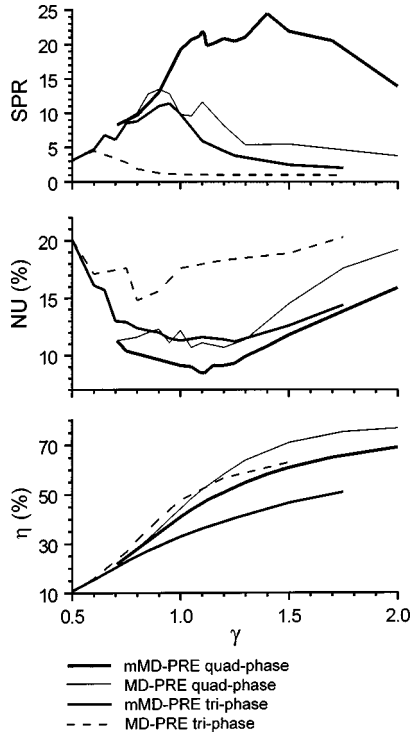

Fig. 11. Simulated performance of blended algorithms as a function of the blending parameter for quantized-phase phase-only modulation characteristics.

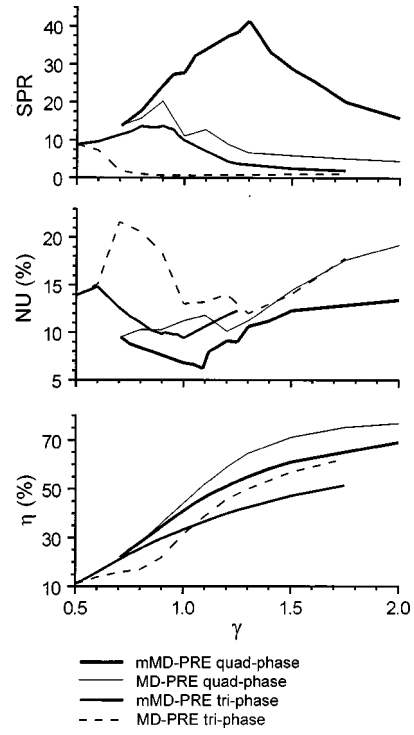

Fig. 12. Simulated performance of blended algorithms as a function of the blending parameter for quantized-phase bi-amplitude phase modulation characteristics.

Table 3. Best Performance of Encoding Algorithms for Bi-Amplitude SLM's

Bi-Amplitude		Simulation			
Algorithm	γ^*	η (%)	SNR	SPR	NU (%)
Tri-phase					
PRE	0.50	11	88	9	14
mMD-PRE	0.90	30	170	14	10
MD-PRE	1.30	50	309	1	12
MDE	1.50	58	366	1	13
Quad-phase					
PRE	0.71	22	197	14	10
mMD-PRE	1.20	51	443	37	8
MD-PRE	1.20	59	606	9	10
MDE	1.20	65	938	5	11

Comparing the quantized biamplitude results with the quantized phase-only results shows that the extra zero-valued state markedly improves the fidelity measures. The diffraction efficiency curves in Figs. 11 and 12 are essentially identical as a function of γ except for the tri-phase MD-PRE curve [which differs because region IV in Fig. 7(a) extends outside the PRE region]. Also, the diffraction efficiency performance reported in Tables 2 and 3 depends directly on the value of γ^* required to optimize the fidelity metrics. Therefore the diffraction efficiency of blended algorithms on phase-only SLM's turns out sometimes to be higher and sometimes to be lower than the efficiency of blended algorithms on biamplitude SLM's.

5. EXPERIMENTAL RESULTS

A. Spatial Light Modulator Characterization and Experimental Procedures

A Boulder Nonlinear Systems Inc. (BNS) 128 × 128-pixel reflective SLM is used in our experiments. BNS normally sells this SLM with ferroelectric liquid crystal (LC). On request they will fill the cell with parallel aligned nematic LC, as was done for us and other groups as well.[29] The relation between voltage and phase modulation has been determined by two methods. One is an interferometric method based on Young's fringes.[30] The second uses the diffraction pattern of a random bi-phase distribution.[8]

For a perfect device the two methods should lead to the same phase characteristic; however, variations in phase response are known to occur across the device.[29] We find experimentally that using the results from the random bi-phase method for phases up to π and from the interferometric method for the range π–2π gives the best correspondence between the actual and an ideal phase-only SLM. For a frequency-doubled Nd-YVO_4 laser (532 nm), we found that a 2π range is produced with 80 electrically addressable gray-scale levels. However, because of the nonlinear transfer curve that is typical for LC SLM's, the phase levels are not equally spaced.

For the measurement of the spot arrays, the linearly polarized laser beam is spatially filtered and collimated. The reflective SLM is uniformly illuminated, with lin-

early polarized light oriented with the extraordinary axis of the LC. The light reflected from the SLM is collected by a Fourier transform lens, and the resulting Fraunhofer diffraction pattern (specifically the zero diffraction order of the SLM grating) is recorded with a Cohu 4915 CCD camera and attached National Instruments black-and-white frame grabber.

After any fixed background noise is subtracted off, the performance metrics are calculated as described in Subsection 2.H with the following exceptions: A noticeable spot, which is due to reflections from the cover glass of the SLM, is always present on the optical axis. It is omitted from all the calculations. The average background noise level is used in calculating not only SNR but also diffraction efficiency η. The average noise level is determined by adding the intensity in several regions (which excludes the undesired on-axis spot and which covers approximately 40% of the total area in the zero order) and then dividing by the area of these regions. The average of the maximum intensity of each of the desired spots is also calculated, and the ratio of the two averages gives SNR. The peak noise spike is found in the identical region that is used for the average noise level calculation. This value of peak noise is used in the calculation of SPR. For diffraction efficiency calculations the average noise level is multiplied by the total area of the zero-order region to estimate the noise energy. This, together with the energy in the desired spots, is considered to be the total energy for purposes of comparing the diffraction efficiency of the experiment with that of the theory.

While calculating efficiency in the above way does provide good agreement between experiment and theory, it is not representative of the physically true efficiency of the BNS SLM. What we find by using a power meter to measure incident and reflected light from the SLM (with all pixels set to gray-scale level 0) is that 1.7% of the energy appears in the on-axis spot, $\sim$5.7% of the energy appears in all diffraction orders (as measured by reimaging the SLM onto the detector of the power meter), and a surprisingly low 0.9% of the energy appears in the zero-order diffraction pattern.

These measurements are aided by a slight lack of parallelism between some of the surfaces in the SLM, which causes the unmodulated spot from the cover glass of the SLM to become spatially resolved from the modulated spot at large distances from the SLM. When a linear phase ramp is programmed on the SLM, we observe that the modulated spot is translated with 95% of its energy present in the translated position and essentially no energy present in the original position. In the higher orders there is also a translated spot, but the unmodulated spot is undetectable. This leads to the conclusion that the unmodulated spot is from a continuous surface that has no spatially varying modulation. That is to say, there is no additional contribution to the unmodulated spot from the dead zones between the pixels. This is further supported by images of the SLM in the phase-only configuration that show dark lines between the pixels. However, in the amplitude-modulating configuration, when viewed through crossed polarizers, the dead zones are bright, which shows that they rotate the polarization.

Also, the losses cannot be attributed entirely to pixel fill factor. BNS quotes the pixel fill factor of a typical device as 60%, and we measured a 54% fill factor when viewing images of the SLM under incoherent illumination. Fill factors in this range indicate that between 29% and 36% of the modulated reflection should appear in the zero order. Therefore we conclude that there are losses of more than 1 order of magnitude in the LC cell.

B. Performance of the Encodings

The phase-only designs summarized in Tables 1 and 2 are implemented with the phase-only SLM, and the measured performance is reported in parentheses in the tables. The measured diffraction efficiencies and SNR are usually quite close, though somewhat less than the simulated values. There are larger deviations between the simulated and measured SPR and NU, with measured SPR usually being smaller and measured NU usually being larger than the simulated values. The measured values still demonstrate the advantages of the modified blended algorithm over the conventional blended algorithm, even though these differences are more difficult to see. In terms of SPR, for the tri-phase SLM the measured differences for the two types of blending are much less than predicted. The differences are much more pronounced for the quad-phase SLM. The situation is reversed for NU. There appears to be a floor to NU of 14%, and so for the quad-phase SLM, which is predicted to produce more uniform patterns, NU is only slightly different between the two blended algorithms. However, for the tri-phase SLM, NU is much larger for PRE and MDE, and this increase in NU is clearly seen in the measurements.

Since the experimental and simulated measurements of performance differ, it could be the case that the optimal performance occurs for different values of γ. This is explored for the case of mMD-PRE on a quad-phase phase-only SLM (Fig. 13). The performance measurements are compared with the simulated results (originally plotted in Fig. 11). Figure 13 shows that the measured diffraction efficiency is somewhat lower than the simulated, the measured NU is higher than the simulated, and the measured SPR is usually lower than the simulated. The shape of each measured curve is quite similar, which suggests that for our experimental SLM the simulated value of γ^* will be reasonably close to the optimal value of γ for experimental settings. While much closer agreement between measurement and theory has been demonstrated with fixed-pattern diffractive optics,[31] we believe that these results are in quite close agreement for programmable SLM's, which suffer from inaccuracies in setting the SLM phase identically on each pixel.[28] Also, interference effects that are due to multiple reflections from the SLM layers and other optical surfaces in the optical system can influence the measurements, especially in the case of NU measurements.[31]

One other possible source of discrepancy between theory and experiment for the NU measurements is the nonuniformity introduced by the frequency roll-off that is due to the subapertures of the SLM pixels. Since the desired portion of the diffraction pattern is along a diagonal, the intensity roll-off is proportional to $\mathrm{sinc}^4(x)$. We find that the closest correspondence between the simulated

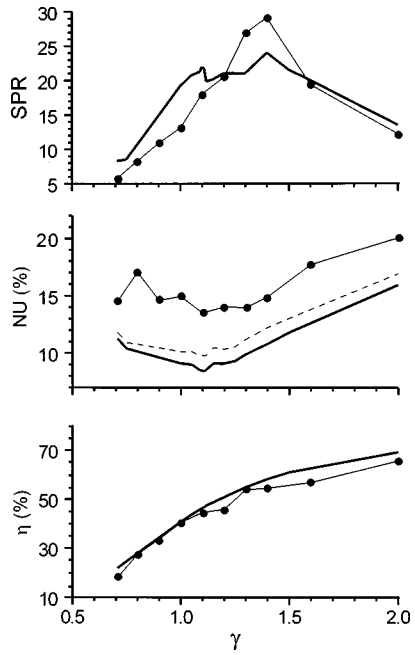

Fig. 13. Comparison between theory (thick solid curve) and experiment (thin solid curve and dots) of the performance of mMD-PRE on quad-phase phase-only SLM's. The dashed curve on the plots of NU shows the theory with the frequency response roll-off (which is to the aperture of the SLM pixels) taken into account.

and the experimentally measured NU occurs if a square pixel aperture of 56% fill factor is used to simulate the pixel-induced rolloff of the originally simulated diffraction pattern. For the particular design considered here, the intensity at the spot location furthest from the optical axis [i.e., the (7, 7) position] is reduced by 16% from the intensity at the spot that is closest to the optical axis. We find that recalculating NU with the additional roll-off would have increased NU by only 0.5%–1.5% over the results reported in Tables 1 and 2 for phase-only and quantized phase-only SLM's. Similarly, recalculated values of NU are plotted in Fig. 13 (dashed curve).[32] While theory and experiment are brought into closer agreement, the other factors considered above still appear to be the dominant sources of error.

6. CONCLUSIONS

A. Summary of Results

We have described and compared two possible ways of combining minimum-distance encoding (MDE) with pseudorandom encoding (PRE). The new modified approach maps the desired value to the closest value that can be achieved by pseudorandom encoding. Simulations with four types of coarsely quantized SLM characteristics clearly show that the modified blended algorithm mMD-PRE outperforms the conventional algorithm MD-PRE in fidelity as measured by peak levels of background noise across the full SBWP of the SLM and by the uniformity of the desired spot array.

Blending by either approach leads to significant improvements in performance over that originally reported in Ref. 24 for PRE and MDE used individually. Especially significant is the 2×–3× increase in diffraction efficiency over that with PRE alone as a result of blending. It is even possible to increase diffraction efficiency over the values reported for best fidelity (i.e., the result for γ^*) by trading off uniformity and SPR as controlled by the scaling parameter γ.

The experimentally implemented designs always showed that the modified blending outperformed the conventional blending, though the differences are not always as evident in all cases studied. This is attributed in large part to errors in controlling the phase of each SLM pixel identically. However, the measured diffraction patterns match the simulated diffraction patterns much more closely than was previously possible by using an optically addressed SLM in Ref. 22. The earlier SLM produced undesired noise orders because of its nonlinear properties and increased nonuniformity of the spot arrays because of its limited resolution. With these limitations absent, the spot arrays are more uniform and the background noise orders are primarily associated with the encoding algorithms and SLM quantization. A further desirable improvement in SLM's would be reduction of the on-axis spot that is due to reflections from the cover and the interfaces of the SLM and that is accentuated by the low-efficiency reflectance of modulated light. Even though further improvements in SLM's are desirable, these experimental results do demonstrate that the encoding algorithms proposed here perform in a manner quite similar to the simulations, thus making the algorithms suitable for use in real-time systems.

B. Implications for Future Research

While blended algorithms tend to improve the optical performance of SLM-based systems over the unblended PRE algorithms, there is additional overhead. Specifically, a search is required to find the optimal scaling parameter γ^*. At this time the only known way to perform this search numerically involves repeated fast-Fourier-transform-based simulations. Additional studies on encoding various functions could possibly lead to the development of a knowledge base that would provide a good *a priori* estimate of the optimal value γ^*. Alternatively, it may be possible to develop theoretical models of the performance of the encoding algorithms as a function of γ. A third possibility would be the inclusion in the optical system of an image sensor that records the far-field pattern and evaluates the performance on line. This would permit much faster evaluation and, as Fig. 13 illustrates, the *in situ* measurements could be used to compensate for the nonideal behavior and other vagaries of current SLM's.

In Section 4 we briefly considered trading off fidelity to increase diffraction efficiency. We achieved this by increasing the value of the blending parameter to increase the amount of MDE in the mMD-PRE algorithm. Additional trade-offs that favor diffraction efficiency can be envisioned by blending the conventional and modified MD-PRE algorithms. The proposed blending could be geometrically interpreted (see Fig. 1) as a mapping from the desired value $\mathbf{a}_c$ to a point on the exterior of the PRE (striped) region. The mapping can be considered a linear combination of the modified and conventional minimum-distance mappings. The actual implementation could be performed in at least two ways: (1) The value/point that

$\mathbf{a}_c$ is mapped to is pseudorandom encoded. (2) The modified and conventional encodings are randomly selected so that the value that $\mathbf{a}_c$ is mapped to is realized on average. Further analysis is required to determine if these approaches actually provide a second trade-off parameter in addition to γ or if one or both of these are alternative interpretations of mMD-PRE. Certainly, such studies may prove valuable, since Figs. 11 and 12 show that for the same value of γ the diffraction efficiency for MD-PRE is as much as 0.15 greater than the efficiency for mMD-PRE, especially when diffraction efficiency has a much higher premium than fidelity.

In conclusion, the performance of Fourier transform holograms from coarsely quantized SLM's can be significantly improved over minimum-distance, pseudorandom, and conventional blended encoding by instead using algorithms that blend pseudorandom encoding with modified minimum-distance encoding. While the new blended algorithm does not outperform blended algorithms for continuous-value phase-only SLM's, it may well be adequate to use coarse quantized SLM's in place of continuous SLM's in a number of applications. These algorithms may be especially useful for SLM developers because they permit early testing and evaluation with prototype devices that have greatly simplified and much less costly electrical addressing circuitry.

ACKNOWLEDGMENTS

This study was supported by Office of Naval Research grant N00014-96-1-1296, NASA cooperative agreement NCC5-222, and the Kentucky Space Grant Consortium.

Address correspondence to Robert W. Cohn at the location on the title page or by phone, 502-852-7077; fax, 502-852-1577; or e-mail, rwcohn@louisville.edu.

REFERENCES AND NOTES

1. N. C. Gallagher and B. Liu, "Method for computing kinoforms that reduces image reconstruction error," Appl. Opt. **12**, 2328–2335 (1973).
2. H. Stark, W. C. Catino, and J. L. LoCicero, "Design of phase gratings by generalized projections," J. Opt. Soc. Am. A **8**, 566–571 (1991).
3. M. P. Dames, R. J. Dowling, P. McKee, and D. Wood, "Efficient optical elements to generate intensity weighted spot arrays: design and fabrication," Appl. Opt. **30**, 2685–2691 (1991).
4. J. Bengtsson, "Kinoform design with an optimal-rotation-angle method," Appl. Opt. **33**, 6879–6884 (1994).
5. E. G. Johnson and M. A. Abushagur, "Microgenetic-algorithm optimization methods applied to dielectric gratings," J. Opt. Soc. Am. A **12**, 1152–1160 (1995).
6. J. N. Mait, "Understanding diffractive optic design in the scalar domain," J. Opt. Soc. Am. A **12**, 2145–2158 (1995).
7. J. N. Mait, "Diffractive beauty," Opt. Photon. News **9**, 21–25 (November 1998).
8. R. W. Cohn and M. Liang, "Pseudorandom phase-only encoding of real-time spatial light modulators," Appl. Opt. **35**, 2488–2498 (1996).
9. R. W. Cohn, A. A. Vasiliev, W. Liu, and D. L. Hill, "Fully complex diffractive optics via patterned diffuser arrays," J. Opt. Soc. Am. A **14**, 1110–1123 (1997).
10. B. R. Brown and A. W. Lohmann, "Complex spatial filter," Appl. Opt. **5**, 967–969 (1966).
11. W.-H. Lee, "Computer-generated holograms: techniques and applications," in *Progress in Optics*, E. Wolf, ed. (Elsevier, Amsterdam, 1978), Vol. 16, pp. 119–231.
12. W. J. Dallas, "Computer-generated holograms," in *The Computer in Optical Research*, B. R. Frieden, ed. (Springer, Berlin, 1980), Chap. 6, pp. 291–366.
13. R. W. Cohn and L. G. Hassebrook, "Representations of fully complex functions on real-time spatial light modulators," in *Optical Information Processing*, F. T. S. Yu and S. Jutamulia, eds. (Cambridge U. Press, Cambridge, UK, 1998), Chap. 15, pp. 396–432.
14. R. W. Cohn and W. Liu, "Pseudorandom encoding of fully complex modulation to bi-amplitude phase modulators," in *Diffractive Optics and Micro-optics*, Vol. 5 of 1996 OSA Technical Digest Series (Optical Society of America, Washington, D.C., 1996), pp. 237–240.
15. L. G. Hassebrook, M. E. Lhamon, R. C. Daley, R. W. Cohn, and M. Liang, "Random phase encoding of composite fully complex filters," Opt. Lett. **21**, 272–274 (1996).
16. R. W. Cohn and M. Liang, "Approximating fully complex spatial modulation with pseudorandom phase-only modulation," Appl. Opt. **33**, 4406–4415 (1994).
17. R. D. Juday, "Optimal realizable filters and the minimum Euclidean distance principle," Appl. Opt. **32**, 5100–5111 (1993).
18. R. W. Cohn, "Pseudorandom encoding of fully complex functions onto amplitude coupled phase modulators," J. Opt. Soc. Am. A **15**, 868–883 (1998).
19. J. P. Kirk and A. L. Jones, "Phase-only complex-valued spatial filter," J. Opt. Soc. Am. **61**, 1023–1028 (1971).
20. L. B. Lesem, P. M. Hirsch, and J. A. Jordon, Jr., "The kinoform: a new wavefront reconstruction device," IBM J. Res. Dev. **13**, 150–155 (1969).
21. J. L. Horner and P. D. Gianino, "Phase-only matched filtering," Appl. Opt. **23**, 812–816 (1984).
22. R. W. Cohn and M. Duelli, "Ternary pseudorandom encoding of Fourier transform holograms," J. Opt. Soc. Am. A **16**, 71–84 (1999).
23. M. W. Farn and J. W. Goodman, "Optimal maximum correlation filter for arbitrarily constrained devices," Appl. Opt. **28**, 3362–3366 (1989).
24. R. D. Juday, "Correlation with a spatial light modulator having phase and amplitude cross coupling," Appl. Opt. **28**, 4865–4869 (1989).
25. M. Montes-Usategui, J. Campos, and I. Juvells, "Computation of arbitrarily constrained synthetic discriminant functions," Appl. Opt. **34**, 3904–3914 (1995).
26. R. D. Juday and J. Knopp, "HOLOMED—an algorithm for computer generated holograms," in *Optical Pattern Recognition VII*, D. P. Casasent and T. Chao, eds., Proc. SPIE **2752**, 162–172 (1996).
27. R. W. Cohn, "Analyzing the encoding range of amplitude-phase coupled spatial light modulators," Opt. Eng. **38**, 361–367 (1999).
28. U. Krackhardt, J. N. Mait, and N. Streibl, "Upper bound on the diffraction efficiency of phase-only fanout elements," Appl. Opt. **31**, 27–37 (1992).
29. D. J. Cho, S. T. Thurman, J. T. Donner, and G. M. Morris, "Characteristics of a 128 × 128 liquid crystal spatial light modulator for wave-front generation," Opt. Lett. **23**, 969–971 (1998).
30. A. Bergeron, J. Gauvin, F. Gagnon, D. Gingras, H. H. Arsenault, and M. Doucet, "Phase calibration and applications of a liquid-crystal spatial light modulator," Appl. Opt. **34**, 5133–5139 (1995).
31. M. Duelli, D. L. Hill, and R. W. Cohn, "Frequency swept measurements of coherent diffraction patterns," Appl. Opt. **37**, 8131–8133 (1998).
32. The influence that is due to roll-off may at first seem to be surprisingly small, but calculating the effect of this roll-off on the nonuniformity/standard deviation of the ideally uniform spot array gives NU = 4.2%. The small influence of the rolloff on NU is further explained by the fact that the simulated values of NU are generally greater than 4% and that standard deviations, rather than being additive, add as the square root of the sum of the squares.